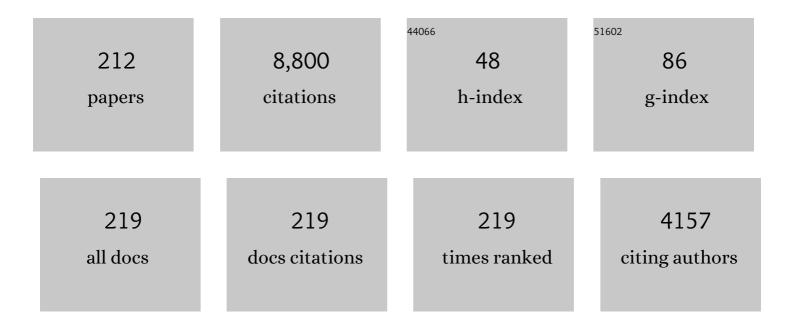
## Tomoo Katsura

List of Publications by Year in descending order

Source: https://exaly.com/author-pdf/1368734/publications.pdf Version: 2024-02-01



Τομοο Κλτευρλ

#	Article	IF	CITATIONS
1	The effect of oxygen fugacity on ionic conductivity in olivine. Geoscience Frontiers, 2022, 13, 101270.	8.4	1
2	Rapid-quenching of high-pressure depolymerized hydrous silicate (peridotitic) glasses. Journal of Non-Crystalline Solids, 2022, 578, 121347.	3.1	5
3	Depressed 660-km discontinuity caused by akimotoite–bridgmanite transition. Nature, 2022, 601, 69-73.	27.8	15
4	Small effect of water incorporation on dislocation mobility in olivine: Negligible creep enhancement and water-induced fabric transition in the asthenosphere. Earth and Planetary Science Letters, 2022, 579, 117360.	4.4	0
5	A Revised Adiabatic Temperature Profile for the Mantle. Journal of Geophysical Research: Solid Earth, 2022, 127, .	3.4	34
6	Extreme conditions research using the large-volume press at the P61B endstation, PETRA III. Journal of Synchrotron Radiation, 2022, 29, 409-423.	2.4	19
7	Water Enhancement of Si Selfâ€Diffusion in Wadsleyite. Journal of Geophysical Research: Solid Earth, 2022, 127, .	3.4	0
8	High pressure-temperature phase relations of basaltic crust up to mid-mantle conditions. Earth and Planetary Science Letters, 2022, 584, 117472.	4.4	18
9	A New Approach Determining a Phase Transition Boundary Strictly Following a Definition of Phase Equilibrium: An Example of the Post-Spinel Transition in Mg2SiO4 System. Minerals (Basel,) Tj ETQq1 1 0.784314	rgB0⊺/Ov	verl <b>o</b> ck 10 T
10	Aluminum solubility in bridgmanite up to 3000Â KÂ at the top lower mantle. Geoscience Frontiers, 2021, 12 929-935.	. 8.4	0
11	Independent hydrogen incorporation in wadsleyite from oxygen fugacity and non-dissociation of H2O in the reducing mantle transition zone. Earth and Planetary Science Letters, 2021, 557, 116755.	4.4	7
12	The grain growth kinetics of bridgmanite at the topmost lower mantle. Earth and Planetary Science Letters, 2021, 561, 116820.	4.4	7
13	Water Solubility in Feâ€Bearing Wadsleyite at Mantle Transition Zone Temperatures. Geophysical Research Letters, 2021, 48, e2021GL092836.	4.0	4
14	High-pressure syntheses and crystal structure analyses of a new low-density CaFe2O4-related and CaTi2O4-type MgAl2O4 phases. American Mineralogist, 2021, 106, 1105-1112.	1.9	3
15	Determination of phase relations of the olivine–ahrensite transition in the Mg2SiO4–Fe2SiO4 system at 1740ÂK using modern multi-anvil techniques. Contributions To Mineralogy and Petrology, 2021, 176, 1.	3.1	4
16	Bridgmanite is nearly dry at the top of the lower mantle. Earth and Planetary Science Letters, 2021, 570, 117088.	4.4	14
17	Direct Viscosity Measurement of Peridotite Melt to Lowerâ€Mantle Conditions: A Further Support for a Fractional Magmaâ€Ocean Solidification at the Top of the Lower Mantle. Geophysical Research Letters, 2021, 48, e2021GL094507.	4.0	7
18	Asthenosphere dynamics based on the H2O dependence of element diffusivity in olivine. National Science Review, 2021, 8, nwaa278.	9.5	5

#	Article	IF	CITATIONS
19	Simultaneous generation of ultrahigh pressure and temperature to 50ÂGPa and 3300ÂK in multi-anvil apparatus. Review of Scientific Instruments, 2021, 92, 103902.	1.3	3
20	A simplified rapid-quench multi-anvil technique. Review of Scientific Instruments, 2021, 92, 113902.	1.3	6
21	Synthesis of paracrystalline diamond. Nature, 2021, 599, 605-610.	27.8	70
22	Pressure Destabilizes Oxygen Vacancies in Bridgmanite. Journal of Geophysical Research: Solid Earth, 2021, 126, .	3.4	5
23	A Novel Highâ€Pressure Tin Oxynitride Sn 2 N 2 O. Chemistry - A European Journal, 2020, 26, 2187-2194.	3.3	9
24	High water solubility of ringwoodite at mantle transition zone temperature. Earth and Planetary Science Letters, 2020, 531, 115987.	4.4	34
25	Boron-doped diamond synthesized by chemical vapor deposition as a heating element in a multi-anvil apparatus. High Pressure Research, 2020, 40, 369-378.	1.2	6
26	A strip-type boron-doped diamond heater synthesized by chemical vapor deposition for large-volume presses. Review of Scientific Instruments, 2020, 91, 095108.	1.3	5
27	A rapid-quench technique for multi-anvil high-pressure-temperature experiments. Review of Scientific Instruments, 2020, 91, 065105.	1.3	11
28	Oxygen Vacancy Substitution Linked to Ferric Iron in Bridgmanite at 27ÂGPa. Geophysical Research Letters, 2020, 47, e2019GL086296.	4.0	8
29	The Effect of Water on Ionic Conductivity in Olivine. Journal of Geophysical Research: Solid Earth, 2020, 125, e2019JB019313.	3.4	22
30	Stability and Solubility of the FeAlO <sub>3</sub> Component in Bridgmanite at Uppermost Lower Mantle Conditions. Journal of Geophysical Research: Solid Earth, 2020, 125, e2019JB018447.	3.4	15
31	Pressure Dependence of Proton Incorporation and Water Solubility in Olivine. Journal of Geophysical Research: Solid Earth, 2020, 125, e2019JB018813.	3.4	8
32	Discovery of Ternary Silicon Titanium Nitride with Spinel-Type Structure. Scientific Reports, 2020, 10, 7372.	3.3	8
33	A Plain Derivation of Birch-Murnaghan Equations of State, and Comparison with Other Equations of State. Review of High Pressure Science and Technology/Koatsuryoku No Kagaku To Gijutsu, 2020, 30, 237-249.	0.0	0
34	Oxygen Vacancy Ordering in Aluminous Bridgmanite in the Earth's Lower Mantle. Geophysical Research Letters, 2019, 46, 8731-8740.	4.0	12
35	Strong correlation of oxygen vacancies in bridgmanite with Mg/Si ratio. Earth and Planetary Science Letters, 2019, 523, 115697.	4.4	14
36	High-pressure synthesis of ultraincompressible hard rhenium nitride pernitride Re2(N2)(N)2 stable at ambient conditions. Nature Communications, 2019, 10, 2994.	12.8	65

#	Article	IF	CITATIONS
37	A new (Mg0.5Fe0.53+)(Si0.5Al0.53+)O3 LiNbO3-type phase synthesized at lower mantle conditions. American Mineralogist, 2019, 104, 1213-1216.	1.9	7
38	Pressure-Induced Emission Enhancement and Multicolor Emission for 1,2,3,4-Tetraphenyl-1,3-cyclopentadiene: Controlled Structure Evolution. Journal of Physical Chemistry Letters, 2019, 10, 5557-5562.	4.6	33
39	Sharp 660-km discontinuity controlled by extremely narrow binary post-spinel transition. Nature Geoscience, 2019, 12, 869-872.	12.9	31
40	A Breakthrough in Pressure Generation by a Kawai-Type Multi-Anvil Apparatus with Tungsten Carbide Anvils. Engineering, 2019, 5, 434-440.	6.7	43
41	Activation of [100](001) slip system by water incorporation in olivine and the cause of seismic anisotropy decrease with depth in the asthenosphere. American Mineralogist, 2019, 104, 47-52.	1.9	5
42	Increase of the oxygen vacancy component in bridgmanite with temperature. Earth and Planetary Science Letters, 2019, 505, 141-151.	4.4	17
43	Hardness of polycrystalline SiO <sub>2</sub> coesite. Journal of the American Ceramic Society, 2019, 102, 2251-2256.	3.8	6
44	A Simple Derivation of the Birch–Murnaghan Equations of State (EOSs) and Comparison with EOSs Derived from Other Definitions of Finite Strain. Minerals (Basel, Switzerland), 2019, 9, 745.	2.0	101
45	Structure, crystal chemistry and compressibility of iron-rich silicate perovskite at pressures up to 95â€GPa. Acta Crystallographica Section A: Foundations and Advances, 2019, 75, e262-e262.	0.1	Ο
46	Complete agreement of the post-spinel transition with the 660-km seismic discontinuity. Scientific Reports, 2018, 8, 6358.	3.3	27
47	Mg lattice diffusion in iron-free olivine and implications to conductivity anomaly in the oceanic asthenosphere. Earth and Planetary Science Letters, 2018, 484, 204-212.	4.4	24
48	Negative activation volume of oxygen self-diffusion in forsterite. Physics of the Earth and Planetary Interiors, 2018, 275, 1-8.	1.9	6
49	Thermal expansion of coesite determined by synchrotron powder X-ray diffraction. Physics and Chemistry of Minerals, 2018, 45, 873-881.	0.8	8
50	Pressure, temperature, water content, and oxygen fugacity dependence of the Mg grain-boundary diffusion coefficient in forsterite. American Mineralogist, 2018, 103, 1354-1361.	1.9	7
51	A nearly zero temperature gradient furnace system for high pressure multi-anvil experiments. High Pressure Research, 2018, 38, 243-249.	1.2	3
52	Experimental determination of melt interconnectivity and electrical conductivity in the upper mantle. Earth and Planetary Science Letters, 2017, 463, 286-297.	4.4	44
53	Identical activation volumes of dislocation mobility in the [100](010) and [001](010) slip systems in natural olivine. Geophysical Research Letters, 2017, 44, 2687-2692.	4.0	5
54	Pressure dependence of transverse acoustic phonon energy in ferropericlase across the spin transition. Journal of Physics Condensed Matter, 2017, 29, 245401.	1.8	6

#	Article	IF	CITATIONS
55	A nearly water-saturated mantle transition zone inferred from mineral viscosity. Science Advances, 2017, 3, e1603024.	10.3	79
56	Phase Relations in the System MgSiO <sub>3</sub> â€Al <sub>2</sub> O <sub>3</sub> up to 2300ÂK at Lower Mantle Pressures. Journal of Geophysical Research: Solid Earth, 2017, 122, 7775-7788.	3.4	40
57	Why and How to Write a Highâ€Impact Review Paper: Lessons From Eight Years of Editorial Board Service to <i>Reviews of Geophysics</i> . Reviews of Geophysics, 2017, 55, 860-863.	23.0	1
58	Pressure generation to 65â€GPa in a Kawai-type multi-anvil apparatus with tungsten carbide anvils. High Pressure Research, 2017, 37, 507-515.	1.2	25
59	Synthesis and crystal structure of LiNbO3-type Mg3Al2Si3O12: A possible indicator of shock conditions of meteorites. American Mineralogist, 2017, 102, 1947-1952.	1.9	14
60	Electrical conductivity of the oceanic asthenosphere and its interpretation based on laboratory measurements. Tectonophysics, 2017, 717, 162-181.	2.2	16
61	Experimental geophysics—measurement of physical and chemical properties of major mantle minerals at high pressures and temperatures. Ganseki Kobutsu Kagaku, 2017, 46, 1-14.	0.1	0
62	Generation of pressures over 40 GPa using Kawai-type multi-anvil press with tungsten carbide anvils. Review of Scientific Instruments, 2016, 87, 024501.	1.3	64
63	Temperature dependence of [100](010) and [001](010) dislocation mobility in natural olivine. Earth and Planetary Science Letters, 2016, 441, 81-90.	4.4	15
64	Si and O self-diffusion in hydrous forsterite and iron-bearing olivine from the perspective of defect chemistry. Physics and Chemistry of Minerals, 2016, 43, 119-126.	0.8	9
65	New constraints on upper mantle creep mechanism inferred from silicon grain-boundary diffusion rates. Earth and Planetary Science Letters, 2016, 433, 350-359.	4.4	41
66	Nucleation process of an M2 earthquake in a deep gold mine in South Africa inferred from onâ€fault foreshock activity. Journal of Geophysical Research: Solid Earth, 2015, 120, 5574-5594.	3.4	23
67	A Complete Solid Solution with Rutileâ€Type Structure in SiO <sub>2</sub> –GeO <sub>2</sub> System at 12ÂGPa and 1600°C. Journal of the American Ceramic Society, 2015, 98, 4111-4116.	3.8	6
68	Heterogeneity of Electrical Conductivity in the Oceanic Upper Mantle. , 2015, , 173-204.		7
69	No effect of water on oxygen selfâ€diffusion rate in forsterite. Journal of Geophysical Research: Solid Earth, 2014, 119, 7598-7606.	3.4	25
70	Electrical conductivity anisotropy in partially molten peridotite under shear deformation. Earth and Planetary Science Letters, 2014, 405, 98-109.	4.4	42
71	Elastic properties of iron-bearing wadsleyite to 17.7GPa: Implications for mantle mineral models. Physics of the Earth and Planetary Interiors, 2014, 228, 92-96.	1.9	30
72	Silicate diffusion in alkali-carbonatite and hydrous melts at 16.5 and 24 GPa: Implication for the melt transport by dissolution–precipitation in the transition zone and uppermost lower mantle. Physics of the Earth and Planetary Interiors, 2013, 225, 1-11.	1.9	30

#	Article	IF	CITATIONS
73	Electrical Conductivity of Mantle Minerals: Role of Water in Conductivity Anomalies. Annual Review of Earth and Planetary Sciences, 2013, 41, 605-628.	11.0	122
74	Small effect of water on upper-mantle rheology based on silicon self-diffusion coefficients. Nature, 2013, 498, 213-215.	27.8	141
75	Crystal structure, Raman and FTIR spectroscopy, and equations of state of OH-bearing MgSiO3 akimotoite. Contributions To Mineralogy and Petrology, 2013, 166, 1375-1388.	3.1	6
76	Single-crystal metastable high-temperature <i>C</i> 2/ <i>c</i> clinoenstatite quenched rapidly from high temperature and high pressure. Acta Crystallographica Section B: Structural Science, Crystal Engineering and Materials, 2013, 69, 541-546.	1.1	5
77	Bond strengths of New Carbon-nitride-Related material C2N2(CH2). Journal of Physics: Conference Series, 2012, 377, 012028.	0.4	3
78	Electrical conductivity of partial molten carbonate peridotite. Physics of the Earth and Planetary Interiors, 2012, 194-195, 1-9.	1.9	48
79	Re-evaluation of electrical conductivity of anhydrous and hydrous wadsleyite. Earth and Planetary Science Letters, 2012, 337-338, 56-67.	4.4	40
80	High silicon self-diffusion coefficient in dry forsterite. Earth and Planetary Science Letters, 2012, 345-348, 95-103.	4.4	67
81	Electrical conductivity of enstatite as a function of water content: Implications for the electrical structure in the upper mantle. Earth and Planetary Science Letters, 2012, 357-358, 11-20.	4.4	52
82	The large-volume press beamline at the extension of PETRA. Acta Crystallographica Section A: Foundations and Advances, 2012, 68, s52-s52.	0.3	0
83	Pressless split-sphere apparatus equipped with scaled-up Kawai-cell for mineralogical studies at 10-20 GPa. American Mineralogist, 2011, 96, 541-548.	1.9	17
84	Phase boundary between perovskite and post-perovskite structures in MnGeO3 determined by in situ X-ray diffraction measurements using sintered diamond anvils. American Mineralogist, 2011, 96, 89-92.	1.9	10
85	Effect of iron content on electrical conductivity of ferropericlase with implications for the spin transition pressure. Journal of Geophysical Research, 2011, 116, .	3.3	42
86	Silicon and magnesium diffusion in a single crystal of MgSiO <sub>3</sub> perovskite. Journal of Geophysical Research, 2011, 116, .	3.3	37
87	High pressure generation using scaled-up Kawai-cell. Physics of the Earth and Planetary Interiors, 2011, 189, 92-108.	1.9	59
88	Variations in electrical conductivity of rocks above metamorphic conditions. Tectonophysics, 2011, 504, 116-121.	2.2	13
89	Ordering in double carbonates and implications for processes at subduction zones. Contributions To Mineralogy and Petrology, 2011, 161, 439-450.	3.1	30
90	Electrical conductivity of dry and hydrous NaAlSi3O8 glasses and liquids at high pressures. Contributions To Mineralogy and Petrology, 2011, 162, 501-513.	3.1	44

#	Article	IF	CITATIONS
91	Systematic study of hydrogen incorporation into Fe-free wadsleyite. Physics and Chemistry of Minerals, 2011, 38, 75-84.	0.8	31
92	Stability and bulk modulus of Ni3S, a new nickel sulfur compound, and the melting relations of the system Ni-NiS up to 10 GPa. American Mineralogist, 2011, 96, 558-565.	1.9	13
93	Crystal Structure of New Carbon–Nitride-Related Material C <sub>2</sub> N <sub>2</sub> (CH <sub>2</sub> ). Japanese Journal of Applied Physics, 2011, 50, 095503.	1.5	13
94	Electrical conductivity of mantle peridotite at the uppermost lower mantle condition. Journal of Physics: Conference Series, 2010, 215, 012102.	0.4	1
95	Synthesis and characterization of strontium–calcium phosphate γ-Ca3â^'xSrx(PO4)2 (0â‰æâ‰⊉). Materials Chemistry and Physics, 2010, 120, 348-350.	4.0	9
96	Electrical conductivity measurements of periclase under high pressure and high temperature. Physica B: Condensed Matter, 2010, 405, 53-56.	2.7	11
97	A Peculiar Site Preference of Boron in MgAl <sub>2–<i>x</i></sub> B <i><sub>x</sub></i> O <sub>4</sub> ( <i>x</i> = 0.0, 0.11, and 0.13) Spinel under Highâ€Pressure and Highâ€TemperatureÂ. Zeitschrift Fur Anorganische Und Allgemeine Chemie, 2010, 636, 472-475.	1.2	8
98	Crystal structure of anhydrous phase X, K1.93(Mg2.02Cr0.02)Si2.00O7. Journal of Mineralogical and Petrological Sciences, 2010, 105, 303-308.	0.9	13
99	Performance of semi-sintered ceramics as pressure-transmitting media up to 30ÂGPa. High Pressure Research, 2010, 30, 443-450.	1.2	36
100	Stishovite single-crystal growth and application to silicon self-diffusion measurements. American Mineralogist, 2010, 95, 135-143.	1.9	28
101	High pressure generation and investigation of the spin transition of ferropericlase (Mg0.83Fe0.17)O. Journal of Physics: Conference Series, 2010, 215, 012099.	0.4	5
102	Pressure–temperature cartography of Fe–S–Si immiscible system. Geochimica Et Cosmochimica Acta, 2010, 74, 3659-3667.	3.9	60
103	Pressure generation and investigation of the post-perovskite transformation in MgGeO3 by squeezing the Kawai-cell equipped with sintered diamond anvils. Earth and Planetary Science Letters, 2010, 293, 84-89.	4.4	43
104	Electrical conductivity of basaltic and carbonatite melt-bearing peridotites at high pressures: Implications for melt distribution and melt fraction in the upper mantle. Earth and Planetary Science Letters, 2010, 295, 593-602.	4.4	113
105	Adiabatic temperature profile in the mantle. Physics of the Earth and Planetary Interiors, 2010, 183, 212-218.	1.9	373
106	Aluminum Nitride Crystal Growth from an Alâ^'N System at 6.0 GPa and 1800 °C. Crystal Growth and Design, 2010, 10, 2563-2570.	3.0	16
107	Electrical conductivity of olivine, wadsleyite and ringwoodite. Ganseki Kobutsu Kagaku, 2009, 38, 33-38.	0.1	0
108	Determination of high-pressure phase equilibria of Fe2O3 using the Kawai-type apparatus equipped with sintered diamond anvils. American Mineralogist, 2009, 94, 205-209.	1.9	29

Tomoo Katsura

#	Article	IF	CITATIONS
109	Water solubility in forsterite at 8–14 GPa. Doklady Earth Sciences, 2009, 425, 432-435.	0.7	9
110	Boron-doped diamond heater and its application to large-volume, high-pressure, and high-temperature experiments. Review of Scientific Instruments, 2009, 80, 023907.	1.3	41
111	The effect of water on the electrical conductivity of olivine aggregates and its implications for the electrical structure of the upper mantle. Earth and Planetary Science Letters, 2009, 288, 291-300.	4.4	194
112	Hydrogen incorporation into forsterite in Mg2SiO4–K2Mg(CO3)2–H2O and Mg2SiO4–H2O–C at 7.5–14.0 GPa. Russian Geology and Geophysics, 2009, 50, 1129-1138.	0.7	12
113	Electrical conductivity of the major upper mantle minerals: a review. Russian Geology and Geophysics, 2009, 50, 1139-1145.	0.7	6
114	Electrical conductivity of wadsleyite as a function of temperature and water content. Physics of the Earth and Planetary Interiors, 2009, 174, 10-18.	1.9	62
115	Thermal expansion of forsterite at high pressures determined by in situ X-ray diffraction: The adiabatic geotherm in the upper mantle. Physics of the Earth and Planetary Interiors, 2009, 174, 86-92.	1.9	39
116	Effect of iron content on electrical conductivity of ringwoodite, with implications for electrical structure in the transition zone. Physics of the Earth and Planetary Interiors, 2009, 174, 3-9.	1.9	43
117	Texture of (Mg,Fe)SiO3 perovskite and ferro-periclase aggregate: Implications for rheology of the lower mantle. Physics of the Earth and Planetary Interiors, 2009, 174, 138-144.	1.9	39
118	A new 6-axis apparatus to squeeze the Kawai-cell of sintered diamond cubes. Physics of the Earth and Planetary Interiors, 2009, 174, 264-269.	1.9	21
119	Reply to Comments on "Electrical conductivity of wadsleyite as a function of temperature and water content―by Manthilake et al Physics of the Earth and Planetary Interiors, 2009, 174, 22-23.	1.9	21
120	<i>P</i> â€ <i>V</i> â€ <i>T</i> relations of wadsleyite determined by in situ Xâ€ray diffraction in a largeâ€volume highâ€pressure apparatus. Geophysical Research Letters, 2009, 36, .	4.0	27
121	Correction to "P-V-T relations of the MgSiO3perovskite determined by in situ X-ray diffraction using a large-volume high-pressure apparatus― Geophysical Research Letters, 2009, 36, .	4.0	5
122	The temperature-pressure-volume equation of state of platinum. Journal of Applied Physics, 2009, 105, .	2.5	59
123	Single crystal growth of wadsleyite. American Mineralogist, 2009, 94, 1130-1136.	1.9	21
124	Pâ€Vâ€T relations of MgSiO <sub>3</sub> perovskite determined by in situ Xâ€ray diffraction using a largeâ€volume highâ€pressure apparatus. Geophysical Research Letters, 2009, 36, .	4.0	39
125	Deviatoric stress and mean pressure in MgO compressed in a Kawai-type apparatus above 30GPa: Evidence for reduction of deviatoric stress by annealing. Journal of Physics and Chemistry of Solids, 2008, 69, 2261-2264.	4.0	2
126	Precise determination of elastic constants by high-resolution inelastic X-ray scattering. Journal of Synchrotron Radiation, 2008, 15, 618-623.	2.4	28

Томоо Katsura

#	Article	IF	CITATIONS
127	Dry mantle transition zone inferred from the conductivity of wadsleyite and ringwoodite. Nature, 2008, 451, 326-329.	27.8	190
128	In situ X-ray diffraction of pyrolite to 40ÂGPa using Kawai-type apparatus with sintered diamond anvils: possibility for the existence of iron-rich metallic particles in the lower mantle. High Pressure Research, 2008, 28, 351-362.	1.2	4
129	Critical Behavior of the Ferromagnetic Perovskite <mml:math xmlns:mml="http://www.w3.org/1998/Math/MathML" display="inline"&gt;<mml:msub><mml:mi>BaRuO</mml:mi><mml:mn>3</mml:mn></mml:msub>. Physical Review Letters, 2008, 101, 077206.</mml:math 	7.8	48
130	Electrical conductivity of majorite garnet and its implications for electrical structure in the mantle transition zone. Physics of the Earth and Planetary Interiors, 2008, 170, 193-200.	1.9	61
131	No interconnection of ferroâ€periclase in postâ€spinel phase inferred from conductivity measurement. Geophysical Research Letters, 2008, 35, .	4.0	30
132	High-pressure synthesis of the cubic perovskite BaRuO <sub>3</sub> and evolution of ferromagnetism in ARuO <sub>3</sub> (A = Ca, Sr, Ba) ruthenates. Proceedings of the National Academy of Sciences of the United States of America, 2008, 105, 7115-7119.	7.1	171
133	Manufacture of a New 6-axis Apparatus. Review of High Pressure Science and Technology/Koatsuryoku No Kagaku To Gijutsu, 2008, 18, 208-213.	0.0	0
134	Growth of large (1 mm) MgSiO3 perovskite single crystals: A thermal gradient method at ultrahigh pressure. American Mineralogist, 2007, 92, 1744-1749.	1.9	32
135	Electrical conductivity measurement of gneiss under mid- to lower crustal P–T conditions. Tectonophysics, 2007, 434, 93-101.	2.2	26
136	Phase-relation studies of mantle minerals by in situ X-ray diffraction using multianvil apparatus. , 2007, , .		5
137	Electrical conductivity measurements of brucite under crustal pressure and temperature conditions. Earth, Planets and Space, 2007, 59, 645-648.	2.5	21
138	Pressure dependence of electrical conductivity of (Mg,Fe)SiO3 ilmenite. Physics and Chemistry of Minerals, 2007, 34, 249-255.	0.8	33
139	Aluminum substitution mechanisms in perovskite-type MgSiO3: an investigation by Rietveld analysis. Physics and Chemistry of Minerals, 2007, 34, 257-267.	0.8	37
140	Phase boundary between ilmenite and perovskite structures in MnGeO3 determined by in situ X-ray diffraction measurements. Physics and Chemistry of Minerals, 2007, 34, 269-273.	0.8	8
141	Tourmaline breakdown in a pelitic system: implications for boron cycling through subduction zones. Contributions To Mineralogy and Petrology, 2007, 155, 19-32.	3.1	36
142	Mantle, Electrical Conductivity, Mineralogy. , 2007, , 684-688.		1
143	Hydrous olivine unable to account for conductivity anomaly at the top of the asthenosphere. Nature, 2006, 443, 973-976.	27.8	258
144	Equation of state of (Mg0.8,Fe0.2)2SiO4ringwoodite from synchrotron X-ray diffraction up to 20 GPa and 1700 K. European Journal of Mineralogy, 2006, 18, 523-528.	1.3	3

#	Article	IF	CITATIONS
145	Electrical conductivity ofFeTiO3ilmenite at high temperature and high pressure. Physical Review B, 2006, 73, .	3.2	19
146	Temperature dependence of the elastic moduli of ringwoodite. Physics of the Earth and Planetary Interiors, 2005, 148, 353-359.	1.9	19
147	Decomposition of brucite up to 20 GPa: evidence for high MgO-solubility in the liquid phase. European Journal of Mineralogy, 2005, 17, 261-267.	1.3	15
148	High-pressure generation in the Kawai-type apparatus equipped with sintered diamond anvils: application to the wurtzite–rocksalt transformation in GaN. , 2005, , 451-460.		11
149	High-pressure generation in the Kawai-type apparatus equipped with sintered diamond anvilsApplication to the wurtzite-rocksalt transformation in GaN. , 2005, , 451-460.		2
150	Computer Control and Measurement Systems for "SPEED-1500", a Kawai-type Multi-anvil Press for in situ X-ray Observations with Synchrotron Radiation. Review of High Pressure Science and Technology/Koatsuryoku No Kagaku To Gijutsu, 2005, 15, 9-14.	0.0	4
151	Recent progress in large-volume high P-T in situ X-ray observation at SPring-8. Acta Crystallographica Section A: Foundations and Advances, 2005, 61, c134-c134.	0.3	0
152	The temperature-pressure-volume equation of state of .GAMMAMg2SiO4. Journal of Mineralogical and Petrological Sciences, 2004, 99, 72-75.	0.9	1
153	Electrical conductivity measurement of granulite under mid- to lower crustal pressure-temperature conditions. Geophysical Journal International, 2004, 157, 79-86.	2.4	72
154	Phase transition of zircon at high P-T conditions. Contributions To Mineralogy and Petrology, 2004, 147, 505-509.	3.1	46
155	Temperature derivatives of elastic moduli of MgSiO3perovskite. Geophysical Research Letters, 2004, 31,	4.0	17
156	Temperature dependence of elastic moduli of β-(Mg, Fe)2SiO4. Geophysical Research Letters, 2004, 31, .	4.0	25
157	Olivine-wadsleyite transition in the system (Mg,Fe)2SiO4. Journal of Geophysical Research, 2004, 109, .	3.3	272
158	Thermal expansion of Mg2SiO4ringwoodite at high pressures. Journal of Geophysical Research, 2004, 109, .	3.3	39
159	Connectivity of molten Fe alloy in peridotite based on in situ electrical conductivity measurements: implications for core formation in terrestrial planets. Earth and Planetary Science Letters, 2004, 222, 625-643.	4.4	80
160	A large-volume high-pressure and high-temperature apparatus for in situ X-ray observation, â€~SPEED-Mk.Il'. Physics of the Earth and Planetary Interiors, 2004, 143-144, 497-506.	1.9	126
161	Melting experiments of mantle materials under lower mantle conditions with implications for magma ocean differentiation. Physics of the Earth and Planetary Interiors, 2004, 143-144, 397-406.	1.9	93
162	Phase relationships and equations of state for FeS at high pressures and temperatures and implications for the internal structure of Mars. Physics of the Earth and Planetary Interiors, 2004, 143-144, 469-479.	1.9	64

Томоо Katsura

#	Article	IF	CITATIONS
163	Core formation in planetesimals triggered by permeable flow. Nature, 2003, 422, 154-157.	27.8	199
164	In situ X-ray observation of iron using Kawai-type apparatus equipped with sintered diamond: Absence of β phase up to 44 GPa and 2100 K. Geophysical Research Letters, 2003, 30, .	4.0	48
165	Post-spinel transition in Mg2SiO4 determined by high P–T in situ X-ray diffractometry. Physics of the Earth and Planetary Interiors, 2003, 136, 11-24.	1.9	210
166	Single-crystal elasticity of ringwoodite to high pressures and high temperatures: implications for 520 km seismic discontinuity. Physics of the Earth and Planetary Interiors, 2003, 136, 41-66.	1.9	116
167	Determination of the phase boundary between theB1andB2phases in NaCl byin situx-ray diffraction. Physical Review B, 2003, 68, .	3.2	40
168	Detailed Structures of Hexagonal Diamond (lonsdaleite) and Wurtzite-type BN. Japanese Journal of Applied Physics, 2003, 42, 1694-1704.	1.5	43
169	Spinel–garnet lherzolite transition in the system CaO-MgO-Al2O3-SiO2 revisited: an in situ X-ray study. Geochimica Et Cosmochimica Acta, 2002, 66, 2109-2121.	3.9	56
170	Microstructures and structural phase transition in (Mg,Fe)SiO3 majorite. European Journal of Mineralogy, 2002, 14, 7-14.	1.3	5
171	In situObservation of ilmenite-perovskite phase transition in MgSiO3using synchrotron radiation. Geophysical Research Letters, 2001, 28, 835-838.	4.0	83

#	Article	IF	CITATIONS
181	Thermoelastic properties of the high-pressure phase of SnO 2 determined by in situ X-ray observations up to 30 GPa and 1400 K. Physics and Chemistry of Minerals, 2000, 27, 618-622.	0.8	55
182	Melting of portlandite up to 6 GPa. Physics and Chemistry of Minerals, 2000, 27, 367-370.	0.8	4
183	ESR study of a new electron center in synthetic stishovite, a high-pressure polymorph of silica. Applied Magnetic Resonance, 2000, 18, 559-564.	1.2	5
184	Peak effect in critical current density induced by oxygen deficiency in the CuBa2Ca3Cu4O10+l´superconductor. Superconductor Science and Technology, 2000, 13, 930-934.	3.5	9
185	Symmetry change of majorite solid solution in the system Mg <sub>3</sub> Al <sub>2</sub> Si <sub>3</sub> O <sub>12</sub> -MgSiO <sub>3</sub> . American Mineralogist, 1999, 84, 1135-1143.	1.9	45
186	Electrical conductivity of silicate perovskite at lower-mantle conditions. Nature, 1998, 395, 493-495.	27.8	101
187	High-pressure transformation of pyrope (Mg3Al2Si3O12) in a sintered diamond cubic anvil assembly. Geophysical Research Letters, 1998, 25, 821-824.	4.0	75
188	Sound velocities and elastic properties of Fe-bearing wadsleyite and ringwoodite. Journal of Geophysical Research, 1998, 103, 20819-20825.	3.3	146
189	The Postspinel Phase Boundary in Mg2SiO4 Determined by in Situ X-ray Diffraction. Science, 1998, 279, 1698-1700.	12.6	251
190	Post-spinel transition in Fe2SiO4. Geophysical Monograph Series, 1998, , 435-440.	0.1	4
191	Metal/silicate partitioning of Mn, Co, and Ni at high-pressures and high temperatures and implications for core formation in a deep magma ocean. Geophysical Monograph Series, 1998, , 215-225.	0.1	15
192	Post-garnet Transition in the System MgSiO3-Al2O3 Review of High Pressure Science and Technology/Koatsuryoku No Kagaku To Gijutsu, 1998, 7, 122-124.	0.0	7
193	Electrical Conductivity Measurement of Minerals at High Pressures and Temperatures Review of High Pressure Science and Technology/Koatsuryoku No Kagaku To Gijutsu, 1998, 7, 18-21.	0.0	3
194	Element Partitioning Between High Pressure Minerals and the Coexisting Silicate Melt Review of High Pressure Science and Technology/Koatsuryoku No Kagaku To Gijutsu, 1998, 7, 98-100.	0.0	0
195	Phase Transition of (Mg,Fe)SiO3 Majorite Review of High Pressure Science and Technology/Koatsuryoku No Kagaku To Gijutsu, 1998, 7, 116-118.	0.0	0
196	Phase relations of natural phlogopite with and without enstatite up to 8 GPa: implication for mantle metasomatism. Earth and Planetary Science Letters, 1997, 146, 511-526.	4.4	92
197	Thermal diffusivity of periclase at high temperatures and high pressures. Physics of the Earth and Planetary Interiors, 1997, 101, 73-77.	1.9	50
198	Determination of Feâ€Mg partitioning between perovskite and magnesiowüstite. Geophysical Research Letters, 1996, 23, 2005-2008.	4.0	66

#	Article	IF	CITATIONS
199	Thermal diffusivity of olivine under upper mantle conditions. Geophysical Journal International, 1995, 122, 63-69.	2.4	57
200	Reactions between molten iron and silicate melts at high pressure: Implications for the chemical evolution of Earth's core. Journal of Geophysical Research, 1995, 100, 5901-5910.	3.3	67
201	Microstructures in β-Mg1.8Fe0.2SiO4 experimentally deformed at transition-zone conditions. Physics of the Earth and Planetary Interiors, 1994, 86, 69-83.	1.9	45
202	Thermal diffusivity of silica glass at pressures up to 9 GPa. Physics and Chemistry of Minerals, 1993, 20, 201.	0.8	30
203	The large volume multi-anvil press as a highP-T deformation apparatus. Pure and Applied Geophysics, 1993, 141, 579-599.	1.9	47
204	The Large Volume Multi-anvil Press as a High P-T Deformation Apparatus. , 1993, , 579-599.		11
205	Measurement of Thermal Diffusivity at High Pressures and High Temperatures Proceedings of the Japan Academy Series B: Physical and Biological Sciences, 1992, 68, 81-86.	3.8	2
206	Stability of Magnesite under the Lower Mantle Conditions Proceedings of the Japan Academy Series B: Physical and Biological Sciences, 1991, 67, 57-60.	3.8	25
207	Dissolution of Silicon and Oxygen in Molten Iron at High Pressure and Temperature Proceedings of the Japan Academy Series B: Physical and Biological Sciences, 1991, 67, 153-158.	3.8	7
208	Melting and subsolidus phase relations in the MgSiO3MgCO3 system at high pressures: implications to evolution of the Earth's atmosphere. Earth and Planetary Science Letters, 1990, 99, 110-117.	4.4	99
209	A temperature profile of the mantle transition zone. Geophysical Research Letters, 1989, 16, 425-428.	4.0	198
210	The system Mg <sub>2</sub> SiO <sub>4</sub> â€Fe <sub>2</sub> SiO <sub>4</sub> at high pressures and temperatures: Precise determination of stabilities of olivine, modified spinel, and spinel. Journal of Geophysical Research, 1989, 94, 15663-15670.	3.3	633
211	The System MgO-SiO <sub>2</sub> -CO <sub>2</sub> -H <sub>2</sub> O at High Pressure: a Preliminary Investigation of CO <sub>2</sub> Concentration in Mantle Fluids. Geophysical Monograph Series, 0, , 275-281.	0.1	0
212	Rapid decrease of MgAlO2.5 component in bridgmanite with pressure. Geochemical Perspectives Letters, 0, , 12-18.	5.0	32